A Simple Method to Disaggregate Passive-Microwave-Based Soil Moisture

Olivier Merlin, Abdelghani Chehbouni, Jeffrey P. Walker, Rocco Panciera, and Yann Kerr, *Senior Member, IEEE*

***Abstract*—This paper develops two alternative approaches for downscaling a passive-microwave-derived soil moisture. Ground and airborne data collected over the Walnut Gulch experimental watershed during the Monsoon'90 experiment were used to test these approaches. These data consisted of eight micrometeorological stations (METFLUX) and six flights of the L-band Push Broom Microwave Radiometer (PBMR). For each PBMR flight, the 180-m-resolution L-band pixels covering the eight METFLUX sites were first aggregated to generate a 500-m "coarse-scale" passive-microwave pixel. The coarse-scale-derived soil moisture was then downscaled to the 180-m resolution using two different surface soil moisture indexes (SMIs): 1) the evaporative fraction (EF), which is the ratio of the evapotranspiration to the total energy available at the surface; and 2) the actual EF (AEF), which is defined as the ratio of the actual-to-potential evapotranspiration. It is well known that both SMIs depend on the surface soil moisture. However, they are also influenced by other factors such as vegetation cover, soil type, root-zone soil moisture, and atmospheric conditions. In order to decouple the influence of soil moisture from the other factors, a land surface model was used to account for the heterogeneity of vegetation cover, soil type, and atmospheric conditions. The overall accuracy in the downscaled values was evaluated to 3% (vol.) for EF and 2% (vol.) for AEF under cloud-free conditions. These results illustrate the potential use of satellite-based estimates of instantaneous evapotranspiration on clear-sky days for downscaling the coarse-resolution passive-microwave soil moisture.**

***Index Terms*—Downscaling, evaporative fraction (EF), evapotranspiration, passive microwave, surface soil moisture.**

I. Introduction

SOIL MOISTURE is a one state variable that controls several Earth-surface-related processes, including hydrology, meteorology, climate modeling, and agricultural management. It controls the partitioning of rainfall into infiltration and runoff, influencing strongly the response of stream discharge to rainfall events, thus playing a key role in the prediction of erosion and sediment loads in watershed streams and ponds [1]. Soil moisture also controls the partitioning of available energy at the land surface into sensible and latent heat fluxes, influencing the development of an atmospheric boundary layer. Moreover, soil moisture is a key variable for a sustainable management of irrigation water, which consumes about 85% of the total available surface water in arid and semiarid regions [2]. In moisture-limited regions, the soil moisture content has also been used as an indicator of the spatial distribution of precipitation and general plant health [3].

The spatial and temporal dynamics of soil moisture are very complex since they depend on several factors. Besides rainfall and evapotranspiration, they also depend on a variety of surface features such as land cover/land use, topography, and soil type. One way of monitoring this variability is through a dense network of continuous soil moisture observations. While this is possible for a confined experimental area during short periods, the establishment of a continuous *in situ* soil moisture monitoring program worldwide is not practical or economically feasible. Consequently, the only possibility for deriving the spatially distributed soil moisture data required for the applications mentioned above is through the use of satellite observations. Satellite-based soil moisture can be obtained from passive or active microwave sensors through the large contrast between the dielectric properties of liquid water (≈ 80) and that of dry soil (≈ 4), and the resulting variability on dielectric properties of soil–water mixtures as they go from dry to wet ($\approx 4-30$).

Active microwave sensors such as the European satellites ERS-1/2 C-band Synthetic Aperture Radar (SAR), ENVISAT C-band Advanced SAR, and the Canadian C-band RADARSAT-1/2 can provide resolutions from 10 to 100 m over a swath width of 50–500 km. While these meet the spatial requirement for most basin-scale hydrological applications [4], they are significantly affected by surface roughness and vegetation biomass, making the soil moisture retrieval difficult. To date, no operational algorithm is available for soil moisture retrieval from the SAR data with the existing spaceborne sensors [5].

Passive-microwave sensors represent an interesting alternative for monitoring soil moisture [6], with airborne sensors operating at low frequencies (L-band), such as the Push Broom Microwave Radiometer (PBMR) and the Electronically Scanned Thinned Array Radiometer, which are found to be very effective for surface soil moisture inference [7]. The Soil Moisture and Ocean Salinity (SMOS) mission [8], which is the first ever passive-microwave spaceborne sensor operating at L-band, is scheduled for launch by the European Space Agency in 2008. This instrument is based on an innovative 2-D aperture synthesis concept, which will bring new and significant capabilities in terms of multiangular viewing configurations and will allow for simultaneous retrieval of soil moisture and vegetation biomass [9], [10] with a revisit time ranging from one to three days. However, the spatial resolution (pixel size) of these types of sensors is about 40 km, and the use of such coarse spatial

Manuscript received March 8, 2007; revised December 11, 2007. This work was supported by the Australian Research Council under a discovery Grant DP0557543.

O. Merlin, J. P. Walker, and R. Panciera are with the Department of Civil and Environmental Engineering, University of Melbourne, Melbourne, Vic. 3010, Australia (e-mail: omerlin@unimelb.edu.au).

A. Chehbouni and Y. Kerr are with the Centre d'Etudes Spatiales de la Biosphère, 31401 Toulouse Cedex 9, France.

Digital Object Identifier 10.1109/TGRS.2007.914807

resolution data in the field of hydrology is not straightforward [11]. Indeed, the scale at which most hydrological processes are better observed and modeled is less than 1 km [12]. Thus, it is of crucial importance to develop simple and robust procedures to downscale a passive-microwave-based soil moisture from its nominal scale to that needed for hydrologic application and/or watershed management.

In this context, several downscaling approaches with different degrees of complexity have been developed during the last decade. Without going into a comprehensive review of all existing methods, which is beyond the scope of this paper, they can be categorized into three groups:

1) methods based on the use of topography and soil depth information [13];
2) methods based on the combination of passive-microwave data with high spatial resolution active microwave data [14] or optical data such as surface temperature and vegetation index [15];
3) methods based on the combination of coarse-resolution passive-microwave data, with fine-scale optical data and a surface process model [12], [16].

This paper is patterned from the work of Merlin *et al.* [16] but with two fundamental differences: 1) There is no need to have dual angle observations of surface temperature; and 2) a simple energy balance model can be used in place of a complex surface process model. Moreover, two different energy balance approaches are developed and tested for downscaling (disaggregating) the coarse-resolution soil moisture data that can be retrieved from spaceborne L-band radiometry. These two approaches are based on two different soil moisture indexes (SMIs): 1) the evaporative fraction (EF), which is the ratio of the evapotranspiration to the total energy available at the surface; and 2) the actual EF (AEF), which is computed as the ratio of the actual-to-potential evapotranspiration. The hypothesis is that these indexes, which can be computed at fine spatial resolution, can provide an information on the fine-scale distribution of surface soil moisture. The projection technique developed in [16] is then implemented with a surface energy balance model to decouple the effects of external factors (i.e., land cover, soil properties, and meteorological forcing) on the relationships between SMIs and surface soil moisture. Ground and airborne data collected over the Walnut Gulch experimental watershed (WGEW) during the Monsoon'90 experiment are used to test the performance of these two approaches. These data consist of eight micrometeorological stations (METFLUX) and six flights of the L-band PBMR. For each PBMR flight, the 180-m-resolution L-band pixels covering the eight METFLUX sites are first aggregated to generate a ~500-m-resolution "coarse-scale" passive-microwave pixel. The coarse-resolution-derived soil moisture is then downscaled using the two approaches outlined above and evaluated against the ground-based data. The applicability of such downscaling methods to SMOS is then discussed.

II. Monsoon'90 Data

The Monsoon'90 experiment was conducted during the summer of 1990 over the USDA-ARS WGEW in southeastern AZ, USA [17], [18]. The purpose of the experiment was to remotely sense moisture fluxes in a semiarid climate during a dry-down. A network of eight meteorological surface energy flux (METFLUX) stations covering the main study area (about 150 km^2) was situated in grass-dominated and shrub-dominated ecosystems and in the transition zones containing both vegetation types. The data collected at each METFLUX site from Julian days (JDs) 204 to 222 consist of 20-min estimates of the following: 0–5-cm soil moisture, meteorological conditions at screen height including air temperature, relative humidity, wind speed, and solar radiation, surface fluxes composed of net radiation, soil heat flux measured at -5 cm, sensible heat flux, and latent heat flux.

As part of the Monsoon'90 campaign, the NASA PBMR was flown on six flights of the C-130 aircraft during a ten-day period in July and August of 1990 [19]. The objective was to map the surface brightness temperature at a wavelength of 21 cm (L-band) and to infer surface soil moisture from these data. The four beams of PBMR point at $\pm 8^\circ$ and $\pm 24^\circ$ incidence angles with a 3-dB beam width of about 30% of the altitude. For Monsoon'90, the PBMR flights were at an altitude of 600 m, which yielded an instantaneous field of view or spatial resolution of 180 m. Available PBMR data of the Monsoon'90 experiment are nadir H-polarized brightness temperatures. To create the images of the brightness temperature at nadir, the outer beams were corrected for incidence angle effects during each PBMR flight by multiplying them by the ratio of the average of the inner beam to the outer beam on each side [19].

In this paper, a time series of six ~500-m-resolution microwave pixels is generated by aggregating the eight 180-m-resolution PBMR pixels covering the METFLUX stations on each day of PBMR observations. The low-resolution soil moisture is retrieved by using the linear regression of PBMR brightness temperature versus the ground-based 0–5-cm soil moisture derived in [19].

III. Method

The surface soil moisture retrieved from the synthetically derived coarse-scale microwave pixels is downscaled by using two fine-scale SMIs at each of the eight METFLUX sites: 1) the EF and 2) the AEF. The downscaling approaches are based on a linear relationship between the surface soil moisture and the SMI. To decouple the effect of other factors on this relationship, the projection technique in [16] is used in conjunction with a surface energy balance model and surface properties at high resolution. The diagram in Fig. 1 illustrates the different steps and parameters involved in the downscaling procedure.

A. General Approach

Assuming a linear relationship between the surface soil moisture and the SMI, the low-resolution soil moisture value can be downscaled using the anomalies in the SMI from its mean for the same area. Consequently, the high-resolution soil moisture values W_H (subscript $_H$ for high resolution $= 180$ m) can be expressed as

$$W_H = W_{L,\text{obs}} + f_{1,L}\left(\text{SMI}_{H,\text{obs}} - \langle \text{SMI}_{H,\text{obs}} \rangle\right) \qquad (1)$$

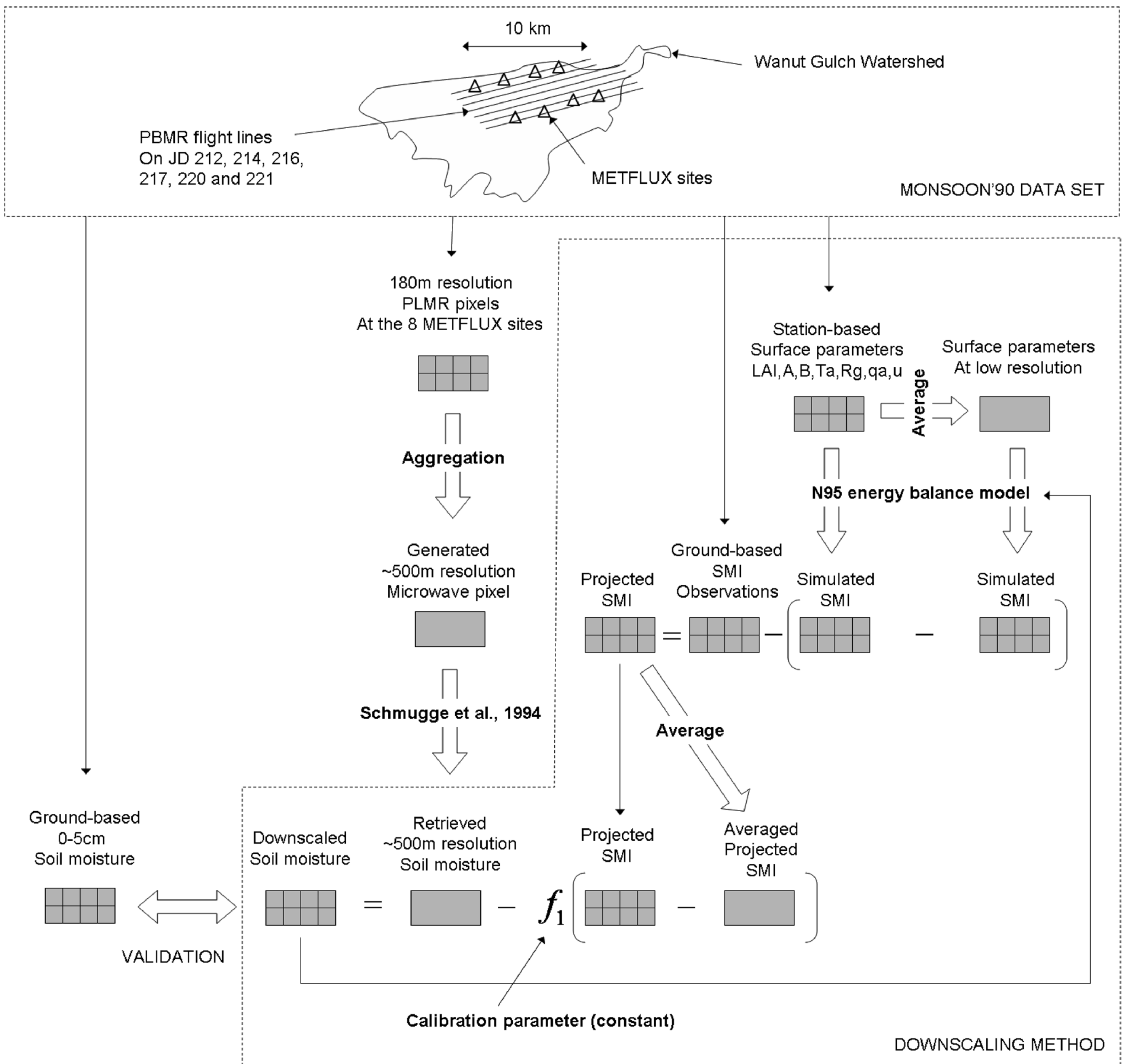

Fig. 1. Schematic diagram of the downscaling procedure.

where $W_{L,\mathrm{obs}}$ (subscript $_L$ for low resolution $= 500$ m and subscript $_{\mathrm{obs}}$ for observed) is the coarse-scale soil moisture that is retrieved from the aggregated PBMR data, $\mathrm{SMI}_{H,\mathrm{obs}}$ is the high-resolution SMI measured at the eight METFLUX sites, $\langle \mathrm{SMI}_{H,\mathrm{obs}} \rangle$ is the SMI averaged at the low resolution, and $f_{1,L}$ (in volume percent) is a scaling parameter used to convert SMI variations into soil moisture variations. In [16], the SMI was the soil temperature inverted from a dual-angle radiative surface temperature, and the slope f_1 was retrieved from SMOS observations by using the multiangular bipolarized information of surface soil emission. As this information may be difficult to extract due to vegetation effects on SMOS observations, this paper tests other SMIs for which the f_1 parameter does not vary much in time and/or can be estimated indirectly from a different source of data. The rationale for choosing EF and AEF as SMIs is that both ratios are, in general, near to constant during the daytime [20]–[24]. Moreover, they are more directly related to surface moisture condition [25] and less dependent on incoming radiation than evapotranspiration or surface temperature [26]. In this paper, parameter f_1 is therefore assumed to be constant in time. As it is also constant in space within the microwave pixel (hypothesis of linearity of the correlation between the SMI and surface soil moisture), the slope f_1 is assumed to be a constant. In this paper, it is calibrated using ground-based data during a training period.

B. SMIs

Herein, EF and AEF are both calculated from the surface fluxes and meteorological data measured at the eight

METFLUX sites. However, they could also be estimated from spaceborne optical sensors [27]–[29]. The observed EF is calculated as

$$\mathrm{EF_{obs}} = \frac{\mathrm{LE_{obs}}}{\mathrm{Rn_{obs}} - G_{\mathrm{obs}}} \tag{2}$$

where $\mathrm{LE_{obs}}$ is the latent heat flux, $\mathrm{Rn_{obs}}$ is the net radiation, and G_{obs} is the ground flux. The observed AEF is calculated as

$$\mathrm{AEF_{obs}} = \frac{\mathrm{LE_{obs}}}{\mathrm{LEp_{obs}}} \tag{3}$$

where $\mathrm{LEp_{obs}}$ is the potential evapotranspiration computed with the Penman–Monteith formula

$$\mathrm{LEp_{obs}} = \frac{\Delta(\mathrm{Rn_{obs}} - G_{\mathrm{obs}}) + \rho C_p \left(\frac{e_s - e_{a,\mathrm{obs}}}{r_{a,\mathrm{obs}}}\right)}{\Delta + \gamma\left(1 + \frac{r_{\min}}{r_{a,\mathrm{obs}}}\right)} \tag{4}$$

where $e_s - e_{a,\mathrm{obs}}$ represents the vapor pressure deficit of the air, ρ is the mean air density at constant pressure, Cp is the specific heat of the air, Δ is the slope of the saturation vapor pressure versus temperature relationship, γ is the psychrometric constant, $r_{a,\mathrm{obs}}$ is the aerodynamic resistance, and $r_{\min}$ is the minimum surface resistance (fixed to $20\ \mathrm{m \cdot s^{-1}}$ for this application). The canopy height used to calculate the aerodynamic resistance is taken from [30].

As an illustration of the dependence of EF to surface soil moisture, Fig. 2 shows the time series of surface soil moisture and EF measured at the METFLUX stations. Both the maximum and minimum values measured at the eight METFLUX stations are plotted to illustrate the range of spatial variability observed within the coarse-scale microwave pixel. The difference between the maximum and minimum surface soil moistures varies from approximately 10% to 20% vol. from JDs 212 to 221. Data are consistent with a presumed correlation between EF and surface soil moisture between 10 am and 2 pm. The difference between the maximum and minimum values of EF generally ranges between 0.2 and 0.5. Note that the values of EF greater than one are due to the presence of clouds, which make the available energy suddenly decrease while the surface is still evaporating.

To assess the link between SMIs and the surface soil moisture over a wider range of moisture and vegetation conditions, the results of a synthetic study are presented in Fig. 3. The surface energy balance model in [31] is used to simulate the variation of both the EF and AEF in response to the surface soil moisture ranging from 0% to 35% vol. and for LAI values varying from zero to four. Atmospheric forcing is fixed (air temperature Ta $= 20$ °C; incoming radiation Rg $= 900\ \mathrm{W \cdot m^{-2}}$; relative humidity qa $= 50\%$; wind speed $u = 3\ \mathrm{m \cdot s^{-1}}$), and surface parameters are set as in [31]. The relationship between the SMI and surface soil moisture is found to be approximately linear below 20% (vol.) but saturates above this threshold. The synthetic study also shows that the soil moisture sensitivity of the SMI decreases with increasing LAI values.

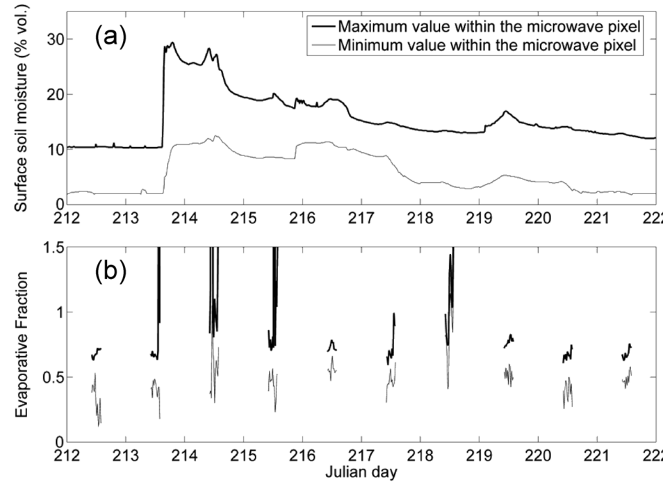

Fig. 2. Time series of the (a) minimum and maximum surface soil moisture observed at the eight METFLUX sites and the (b) minimum and maximum EF measured at the eight METFLUX sites between 10 am and 2 pm from JDs 212 to 221.

C. Projection

The basis for the projection step is to improve the relationship between the SMI and the surface soil moisture used for downscaling the low-resolution soil moisture in (1). The methodology used in this paper is that developed in [16] (but the SMI used is different as discussed above). It consists of using a land surface model to simulate the impact of surface parameters, such as vegetation cover, soil type, and atmospheric conditions, on the relationship between the SMI and surface soil moisture at high resolution. In this application, the surface energy balance model is used to simulate EF or AEF at a high resolution given: 1) surface parameters available at high resolution and 2) the same set of surface parameters averaged at low resolution. The projected SMI, which is denoted as $\overline{\mathrm{SMI}_{H,\mathrm{obs}}}$, is the observed SMI that is less than the difference of the two simulated SMIs

$$\overline{\mathrm{SMI}_{H,\mathrm{obs}}} = \mathrm{SMI}_{H,\mathrm{obs}} - [\mathrm{SMI}_{H,\mathrm{sim}}(W_H, p_H) - \mathrm{SMI}_{H,\mathrm{sim}}(W_H, \langle p \rangle_H)] \tag{5}$$

where $\mathrm{SMI}_{H,\mathrm{sim}}(W_H, p_H)$ (subscript $_{\mathrm{sim}}$ indicates simulated) is the SMI simulated using the modeled soil wetness and surface parameters p at high resolution, and $\mathrm{SMI}_{H,\mathrm{sim}}(W_H, \langle p \rangle_H)$ is the simulated SMI using the modeled surface wetness and surface parameters averaged at the microwave resolution. The projected SMI is therefore a combination of the observed SMI and the SMI simulated at fine scale by a surface energy model using fine-scale and aggregated parameters. Note that the projection does not require all the surface parameters involved in the surface energy budget (input of the model) to be available at high resolution. If one parameter is available at high resolution (vegetation cover for instance), the projection can be applied with respect to this parameter only.

By replacing the observed SMI with the projected SMI, (1) becomes

$$W_H = W_{L,\mathrm{obs}} + f_{1,L}\left(\overline{\mathrm{SMI}_{H,\mathrm{obs}}} - \langle \overline{\mathrm{SMI}_{H,\mathrm{obs}}} \rangle\right). \tag{6}$$

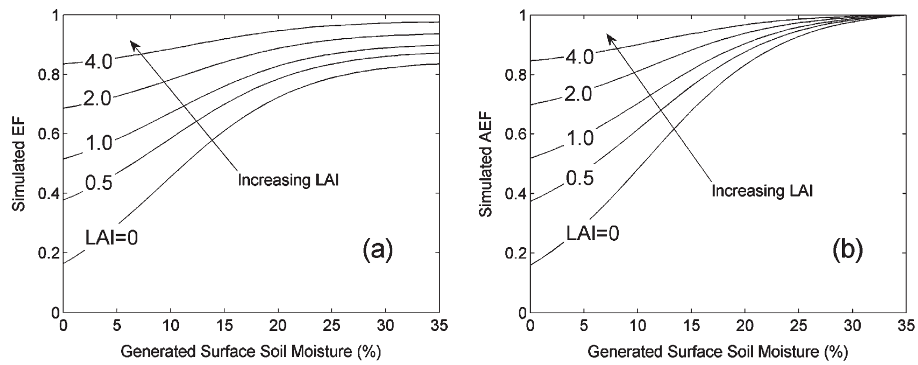

Fig. 3. Sensitivity of the (a) simulated EF and the (b) simulated AEF to surface soil moisture for increasing LAI values.

Note that the application of (6) requires iterating on soil moisture values, as W_H is not known at the beginning of the procedure. In fact, the algorithm runs a loop on integer k with

$$W_{H,k} = W_{L,\mathrm{obs}} \tag{7}$$

for $k = 0$ (initialization) and

$$W_{H,k} = W_{L,\mathrm{obs}} + f_{1,L}\left(\overline{\mathrm{SMI}(W_{H,k-1})} - \left\langle\overline{\mathrm{SMI}(W_{H,k-1})}\right\rangle\right) \tag{8}$$

for $k > 0$. Convergence of W_H within 0.1% vol. is typically reached after two or three iterations on k. Since parameter f_1 is assumed to be constant in time and space (within the microwave pixel), W_H is the only parameter to vary in (8).

D. Land Surface Energy Balance Model

The energy balance model used for the application of this downscaling approach to the Monsoon'90 data is the N95 model developed by Norman *et al.* [31], revised by Kustas *et al.* [32], and further improved by Kustas and Norman [33]. It is a dual-source model which treats the energy balance of the soil/substrate and vegetation using surface skin temperature observations at the zenith view angle [31] and remotely sensed images of near-surface soil moisture [32] for estimating the soil energy balance over the watershed. In this paper, the revised model by Kustas *et al.* [32] is used because the heterogeneity of the 0–5-cm soil moisture is accounted for in the estimation of surface fluxes. The model formulation explicitly computes the soil evaporation as a function of the resistance of the top soil layer to water vapor transfer. The resistance of the surface soil layer r_{ss} is parameterized using a near-surface soil moisture [34]

$$r_{\mathrm{ss}} = \exp(A - BW/W_{\mathrm{sat}}) \tag{9}$$

where A and B are two calibration parameters, and W_{sat} is the soil moisture at saturation (35% vol. for the Walnuch Gulch site). The total net radiation Rn is partitioned into Rns and Rnc as in [28]

$$\begin{cases} \mathrm{Rns} = \mathrm{Rn}\exp(-\kappa \mathrm{LAI}) \\ \mathrm{Rnc} = \mathrm{Rn}\left[1 - \exp(-\kappa \mathrm{LAI})\right] \end{cases} \tag{10}$$

where κ is estimated to be 0.45 for high solar zenith angles.

TABLE I
CALIBRATION PARAMETERS COMPRISED OF THE LEAF AREA INDEX AND TUNING PARAMETERS A AND B OF THE SOIL RESISTANCE TO EVAPORATION AT THE EIGHT METFLUX SITES

Site	LAI	A	B
1	0.4	9	9
2	0.3	8	5
3	0.4	9	8
4	0.4	8	4
5	0.2	8	5
6	0.2	8	5
7	0.7	8	4
8	0.6	8	4

The simulated SMI used in (5) is computed by replacing the observed fluxes in (2) and (3) with the fluxes simulated by the N95 model. Note that the potential latent heat flux is simulated with W_{sat} as input to the energy balance model. The N95 model is calibrated against EF observations during a training period between JDs 206 and 211. The measured and simulated EF is averaged between 10 am and 2 pm, and the root mean square difference between the average of the measured and simulated EF is minimized by varying the parameters A, B, and LAI. Note that the objective here is not to evaluate the model at the METFLUX sites but to derive a simple calibration for further applications. Another calibration approach would have been to use LAI measurements and to adjust coefficient extinction κ. Results of the site-specific calibration are presented in Table I. The space-varying surface parameters p are composed of A, B, LAI, canopy height, air temperature Ta, relative humidity qa, solar radiation Rg, and wind speed u. The other input parameters (albedo, thermal emissivity, κ, and W_{sat}) are fixed to uniform values as in [33].

IV. APPLICATION

The application of the downscaling approaches presented here involves successively as follows: 1) projecting EF and AEF using N95 and (5); 2) estimating the slope f_1 from point scale observations; and 3) downscaling the coarse-resolution

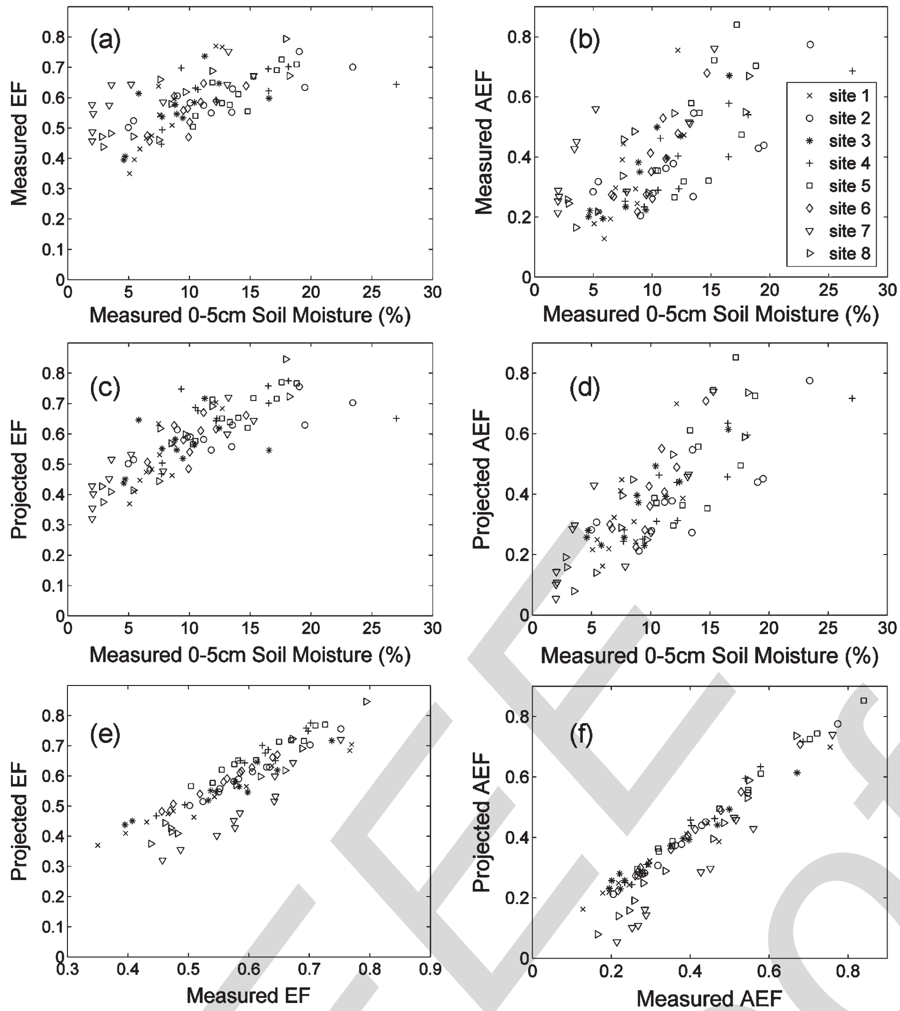

Fig. 4. Measured and projected SMIs versus surface soil moisture observations between JDs 212 and 221. The projected SMIs are also plotted versus measured SMIs for comparison.

soil moisture retrieved from the six generated microwave pixels using (6). The approach is demonstrated using Monsoon'90 data, and the downscaled results are compared with the ground-based measurements.

The projection technique is applied to the data set between JDs 212 and 221. The projected EF and AEF that are calculated using (5) are averaged between 10 am and 2 pm and compared to the 10 am to 2 pm average of the measured EF and AEF from METFLUX stations. Results are presented in Fig. 4, where it is apparent that the relationship between SMI and W is improved by the projection in both cases; the correlation coefficient is increased from 0.66 to 0.79 and from 0.71 to 0.81 for EF and AEF, respectively. The projection is therefore a useful tool to decouple the effect of other variables on the correlation between SMI and W, given that a surface energy model can be properly calibrated over heterogeneous areas, with notably different vegetation cover and soil properties.

The parameter f_1 is calibrated by minimizing the root mean square difference between the soil moisture simulated with (6) and the observations from JDs 206 to 211 (W_L is computed as the average of ground-based observations in this case). The mean and standard deviation of f_1 are evaluated as 56 and 10 and as 47 and 7 for EF and AEF, respectively (f_1 is in volume percent). In our analysis, parameter f_1 is assumed to be a constant through time and space. The same mean value of f_1 obtained between JDs 206 and 211 is subsequently used in the application during PBMR flights from JDs 212 to 221, which follows the calibration period. This allows testing the assumption that f_1 can be held constant by using an independent data set.

The soil moisture retrieved at coarse resolution from the six generated microwave pixels is then downscaled with (6) using the projected SMIs and the estimated value of the slope f_1. The downscaled soil moisture is plotted against the ground-based soil moisture measurements in Fig. 5 for both the EF and AEF approaches. Table II reports the average root mean square error (rmse) between the downscaled and measured soil moisture values for each of the eight subpixels and the six days of data. When using all parameters at high resolution (meteorological data, and soil and vegetation parameters), the average of the rmse is about 2% (vol.) and 3% (vol.) for AEF and EF, respectively. On JD 214, however, the disaggregation error is larger than 5% (vol.) in both cases. The poor agreement with ground observations on JD 214 can be explained by the following: 1) the great variations of f_1 with the presence of clouds (see time series of EF in Fig. 2) and 2) the saturation of

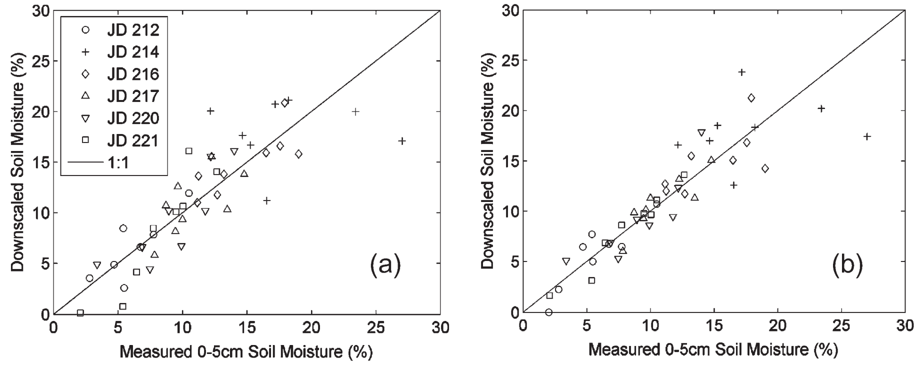

Fig. 5. Downscaled versus measured surface soil moisture for the six microwave pixels generated on JDs 212, 214, 216, 217, 220, and 221. The results obtained with the (a) EF and (b) AEF are compared.

TABLE II
AVERAGE RMSE ON THE DOWNSCALED SURFACE SOIL MOISTURE FOR THE SIX GENERATED MICROWAVE PIXELS. RESULTS OBTAINED WITH EF AND AEF, AND WITH ANCILLARY DATA AVAILABLE AT HIGH OR LOW RESOLUTION, ARE SUCCESSIVELY PRESENTED

	RMSE (% vol.)									
	EF					AEF				
JD	**High-resolution parameters**	Low-resolution meteo data	Low-resolution soil parameters	Low-resolution LAI	Low-resolution canopy height	**High-resolution parameters**	Low-resolution meteo data	Low-resolution soil parameters	Low-resolution LAI	Low-resolution canopy height
212	**1.9**	1.8	2.6	2.5	2.0	**1.2**	1.3	1.9	1.7	1.2
214	**5.6**	5.0	6.3	6.0	6.0	**5.3**	5.3	5.6	5.6	6.2
216	**1.8**	1.9	2.4	3.0	1.7	**2.4**	2.1	2.6	3.1	2.5
217	**2.2**	2.2	1.9	3.8	2.0	**1.2**	1.4	1.4	2.0	1.3
220	**2.2**	1.9	1.8	3.2	2.6	**1.9**	1.5	2.2	2.8	2.0
221	**2.7**	2.3	2.5	2.8	3.0	**1.0**	1.2	1.1	1.9	1.2
Mean	**2.7**	2.5	2.9	3.6	2.9	**2.2**	2.1	2.4	2.8	2.4

SMI for soil moisture values above 20% (vol.) (see synthetic study in Fig. 3).

The comparison of the downscaling results with EF and AEF shows that the AEF-based approach performs the best in most cases. In Table II, the error on the downscaled values is, in general, lower (except on JD 216) when using the AEF. As the N95 model was calibrated against EF observations, and not against AEF observations, results with the EF approach were expected to be superior. While the projection technique improves the correlation between EF and W, as compared to AEF and W, the correlation between the measured AEF and surface soil moisture is simply higher. The stronger link between AEF and surface soil moisture can be explained by several factors.

First, AEF is intrinsically more directly linked to the surface moisture status than EF, as AEF is defined relative to a "wet surface," whereas EF is defined relative to a surface at the "thermal equilibrium." In the case of bare soil in particular, various analyses have shown that AEF can be expressed as a function of solely near-surface soil moisture alone [35], [36]. For vegetated surfaces, AEF is also dependent on vegetation characteristics and water potential in the root zone. However, one can argue that the normalization of AEF at saturation $(\mathrm{AEF} = 1)$ makes this SMI more applicable to different vegetation covers in this range of soil moisture. Fig. 2 shows how AEF scales with the surface soil moisture, which is less dependent on LAI for high soil moisture values than EF.

The second explanation for a stronger link with AEF and soil moisture is that the diurnal variability of EF may limit the validity of the "f_1 constant" hypothesis in this case. The diurnal behavior of EF depends on both surface and atmospheric conditions. Notably, the atmospheric demand for evapotranspiration is governed by solar radiation, relative humidity, and to a lesser extent, air temperature, and wind speed, whereas surface control is exerted by soil moisture and vegetation condition. This issue has been heavily investigated from both experimental and theoretical perspectives [22], [23], [37]. Most of these studies have reported a typical concave-up shape for EF which can induce errors when assuming a daytime constant EF that is equal to the noon value, since the latter is always lower than

TABLE III
AVERAGE AT THE EIGHT METFLUX SITES OF THE RELATIVE DIURNAL VARIABILITY OF EF AND AEF, AND STANDARD DEVIATION OF SOLAR RADIATION, RELATIVE HUMIDITY, AIR TEMPERATURE, AND WIND SPEED EVALUATED BETWEEN 10 AM AND 2 PM FOR EACH DAY BETWEEN JDs 212 AND 222. THE SIX DAYS OF PBMR FLIGHT ARE UNDERLINED

JD	Relative variability (%)		σRg	σqa	σTa	σu
	EF	AEF	(Wm^{-2})	(ºC)	(ºC)	(ms^{-1})
212	26	12	110	3.5	1.0	0.6
213	13	5	74	5.3	1.8	1.0
214	21	28	260	5.7	1.9	0.8
215	20	18	169	4.0	1.7	0.9
216	10	11	101	3.9	1.6	0.6
217	23	12	198	2.8	1.5	1.2
218	31	32	84	7.4	1.7	0.8
219	14	16	133	3.1	1.5	0.6
220	17	11	114	3.9	1.6	0.7
221	13	7	57	5.5	1.8	0.8
222	13	3	54	3.0	1.8	0.8

the daily average [24]. The assumption of the self-conservation of EF during daytime is only valid under relatively dry-surface and clear-sky conditions [21], [37].

To check the stability of both SMIs with the Monsoon'90 data, the relative variability of EF and AEF is estimated by successively calculating the standard deviation of measurements at the eight METFLUX sites between 10 am and 2 pm, averaging the eight standard deviations, and normalizing the diurnal variability with the soil moisture sensitivity of SMIs. The soil moisture sensitivity of AE and AEF is evaluated as the difference between the SMIs calculated at 20% (vol.) (maximum value) and 0 (minimum value) using the linear regression of the EF$-W$ and AEF$-W$ relationships, respectively. Table III lists the values of the relative diurnal variability (in %) of EF and AEF evaluated for each day between JDs 212 and 222. The average diurnal cycle represents about 20% and 15% of the sensitivity to surface soil moisture for EF and AEF, respectively. It is suggested that the superiority of the AEF-based approach is partly due to the relative stability of AEF for changing atmospheric conditions.

Finally, the comparison between the error on the downscaled soil moisture in Table II and the diurnal variation of EF and AEF in Table III indicates that the performance of the disaggregation is well correlated with the stability of SMIs. For example, the disaggregation results are significantly improved on JDs 212, 217, and 221, for which the diurnal variability of AEF is approximately half that of EF. The temporal variability of atmospheric conditions is also presented in Table III for comparison with the diurnal variability of SMIs. The temporal variations of solar radiation, relative humidity, air temperature, and wind speed are calculated as the spatial average at the eight METFLUX sites of the standard deviation between 10 am and 2 pm. It is apparent that variations in EF and AEF can be attributed to the changes in solar radiation and relative humidity, with the impact of air temperature and wind speed being less visible with these data.

V. LIMITATIONS AND APPLICABILITY TO SMOS

The application of the passive-microwave downscaling approach developed in this paper to Monsoon'90 data has demonstrated the potential performance when using ground-based measurements over a limited range of surface conditions (eight locations distributed within a 150-km^2 semiarid area) during a short period of time (20 days). Here, we assess the applicability of the proposed downscaling method to SMOS data, with larger space-time scales. The assumptions underlying the development of (1) to (6) are listed and discussed. A sensitivity analysis of the algorithm is also conducted to evaluate the impact of uncertainties in ancillary data, high-resolution SMI observations, and low-resolution surface soil moisture observations.

A. Assumptions

The methodology is based on five assumptions. Each assumption is stated below and followed by a discussion regarding its applicability to SMOS-like data.

1) Cloud-free conditions: EF observations can be derived at large spatial scales using optical data [27]–[29], but optical data will be available for clear-sky conditions only. Note that clear-sky conditions are also needed, as shown in the application to Monsoon'90, to meet the "f_1 constant" hypothesis. In the context of SMOS, an interpolation between dates could be done on SMI observations in order to apply the downscaling scheme on cloudy days.

2) SMI observations are available at approximately the same time as the passive-microwave observations so that the low-resolution surface soil moisture does not vary much between the two observation types. With daily optical data such as the MODerate resolution Imaging Spectroradiometer (MODIS), this requirement is generally met. One can assume that the 40-km soil moisture typically does not change significantly between 6 am (SMOS overpass time) and 10 am (MODIS overpass time).
3) The SMI is assumed to be linearly correlated to surface soil moisture by (1) and (6). The synthetic study in Fig. 3 showed that the SMI saturates above 20% (vol.) in the case of the Walnut Gulch watershed. The method with f_1 constant (independent of coarse-scale soil moisture) is thus limited to dry-end soil moisture conditions.
4) At least one parameter involved in the surface energy budget, such as vegetation cover, soil properties, and meteorological forcing, is available at high resolution in order to apply the projection technique of (5). In the context of SMOS, vegetation/soil properties can be provided at 1-km resolution from the optical data (e.g., MODIS) and global databases (e.g., ECOCLIMAP [38]).
5) The slope of the relationship between SMI and surface soil moisture f_1 is assumed to be independent of meteorological forcing data. This allows the following.
   a) The use of the projection technique with low-resolution meteorological data only: Such data would be available for global applications (e.g., output from NWP models).
   b) The calibration of f_1 during a training period that is independent from the application data set: Note that the value of f_1 still varies with any changes in vegetation cover. The calibration of f_1 should therefore be undertaken for each microwave pixel and as often as the surface conditions (seasons and land use) change within the microwave pixel. This can be done by comparing the SMI and surface soil moisture observations at low resolution.

B. Sensitivity Analysis

To assess the impact of uncertainties in input data on the downscaling procedure, realistic measurement errors are added to high-resolution SMI and low-resolution surface soil moisture observations. Three cases are investigated.

1) Surface parameters, such as vegetation characteristics (LAI and canopy height), soil properties (A and B), and meteorological data (Rg, Ta, ua, and qa), are available at low resolution only.
2) A bias ranging from -5% to $+5\%$ vol. on the low-resolution soil moisture observation.
3) 10% and 20% random errors on SMI observations with LAI ranging from zero to four.

For each of the three cases, the impact on the downscaled soil moisture is evaluated and discussed.

1) Surface Parameters Available at Low Resolution Only: To evaluate the impact of ancillary data resolution on the downscaling procedure, the same data set as in the previous section is applied but with the surface parameters one-by-one averaged at the scale of the microwave pixel. Table II lists the mean rmse on the downscaled soil moisture obtained for each type of ancillary information separately. Results are to be compared to the case (in bold in the table) where all surface parameters are available at high resolution. It is apparent that the spatial resolution of soil resistance parameters and canopy height (ranging from 0.1 to 0.6 m for Monsoon'90) has no significant impact on the downscaling results. However, the impact of the resolution of LAI is more significant. The mean rmse increased from 2.7% to 3.7% (vol.) for EF and from 2.2% to 2.8% (vol.) for AEF. The impact of the resolution of meteorological data is very low for both EF and AEF. Surprisingly, the downscaling results are slightly better, in general, with low-resolution than with high-resolution atmospheric forcing. It is suggested that the projection is not able to correct the impact of meteorological conditions to the correlation between SMI and surface soil moisture, as this impact is rather small with EF and AEF.

As a summary, the critical ancillary data to be used at high resolution appear to be the LAI and soil parameters. The resolution of meteorological data does not appear to have a significant impact on the downscaling results. Note, however, that the spatial extent of the data set used in this paper is rather small (150 km^2) compared to the SMOS pixel size (1600 km^2), which means that higher heterogeneities are expected at the scale of a SMOS pixel, with potentially higher impacts on the downscaled soil moisture.

2) Bias on the Low-Resolution Surface Soil Moisture Observation: To evaluate the impact of a given bias on the low-resolution surface soil moisture observation to the downscaled soil moisture, a bias of -5% to $+5\%$ vol. in 1% increments is successively added to the low-resolution soil moisture observation. The resulting bias on the downscaled soil moisture W_H is plotted as function of the input bias on W_L in Fig. 6 for EF and AEF separately. It is shown that the mean output bias is practically equal to the input bias, which is a direct reflection of the assumed linear relationship between high- and low-resolution surface soil moistures in (1) and (6). Note that the slight divergence of the high-resolution bias with respect to the 1:1 line for negative biases is due to the negative values of surface soil moisture that were forced to zero in the computations.

3) Uncertainty in Remotely Sensed EF: Space-based estimates of EF are probably more uncertain than the ground-based estimates acquired during a field experiment such as Monsoon'90. The objective is to simulate realistic uncertainties on space-based EF observations and to evaluate its impact on the disaggregation results. A synthetic study is undertaken to quantify the error on the downscaled soil moisture associated with errors of 10% and 20% on SMI estimates and with a LAI ranging from zero to four. Fig. 6 shows the results obtained for EF and AEF separately, showing that an error of 5% vol. is achievable with 10% error on SMI. However, an error of 20% on SMI significantly impacts the downscaled soil moisture with an error estimated to 10% (vol.).

4) Independent Random Errors in Input Data: To test the impact of uncertainty in all input data simultaneously, the

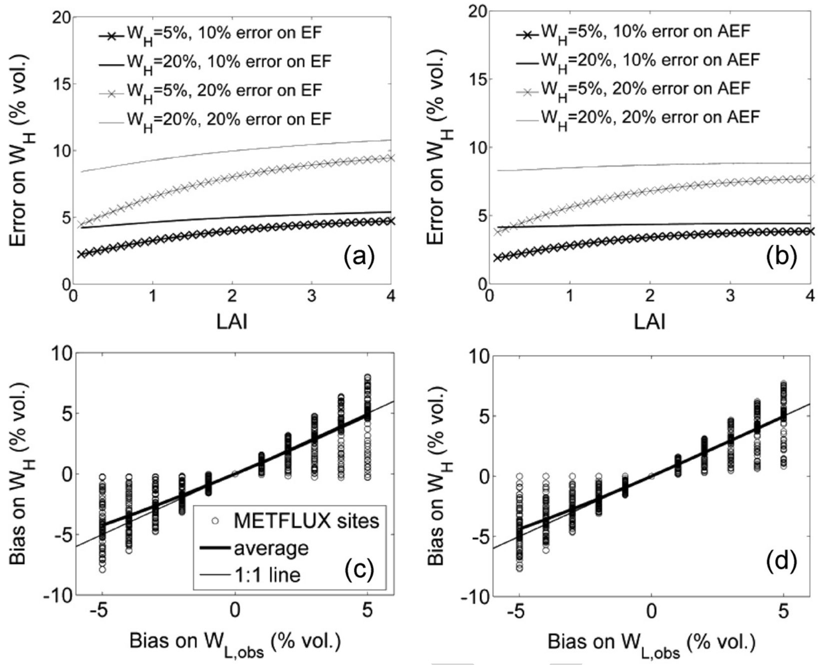

Fig. 6. Estimated error on the downscaled soil moisture associated with a given uncertainty in SMI observations and a given bias on low-resolution soil moisture observations.

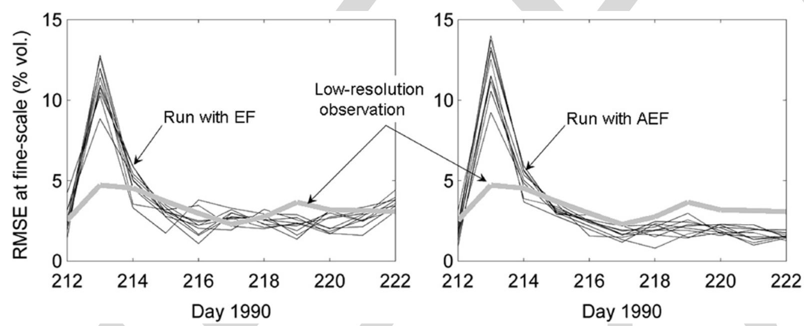

Fig. 7. Estimated error on the downscaled soil moisture associated with simultaneous and independent errors in input data. The error at fine scale of low-resolution soil moisture observation is also plotted for comparison.

downscaling algorithms are run from JDs 212 to 222 with 20% error on EF/AEF, an error on coarse-scale meteorological data that is equal to the standard deviation observed at fine scale, and 4% error on low-resolution soil moisture observation. When PBMR data are not available, a low-resolution soil moisture observation is generated by aggregating high-resolution observations. The results are averaged between 10 am and 2 pm as for the application with real data (with no perturbation) and presented in Fig. 7 for ten independent runs. The aggregation of EF/AEF (in time) between 10 am and 2 pm significantly reduces the uncertainty from about 10% according to previous estimates to about 3% vol. (except on cloudy day 313). The errors on the disaggregated soil moisture are generally smaller than that of the low-resolution soil moisture observation—as compared with high-resolution observations—which indicates that independent random errors on EF/AEF, meteorological data, and low-resolution soil moisture observation generally cancel out in disaggregation products. The different behaviors obtained with EF and AEF and the poor results obtained on JD 213 are consistent with the previous results in Section IV.

VI. Conclusion

Two simple approaches for downscaling (disaggregating) a coarse-resolution passive-microwave-derived soil moisture, as anticipated from SMOS, were developed and tested using ground and airborne data that were collected over the WGEW during the Monsoon'90 experiment. The verification data consisted of eight METFLUX stations and six flights of the L-band PBMR. For each PBMR flight, the L-band pixels covering the eight stations were first aggregated to generate a time series of six ∼500-m coarse-scale passive-microwave pixels. The soil moisture retrieved from the low-resolution microwave observations was then downscaled to 180 m using two different SMIs to describe the subpixel variability of surface soil moisture: 1) the ratio of the evapotranspiration to the available energy (EF) and 2) the ratio of the actual-to-potential evapotranspiration (AEF). It is well known that both SMIs depend on surface soil moisture. However, they are also influenced by other factors such as vegetation cover, soil type, and atmospheric conditions. In order to decouple the influence of soil moisture from the other factors, a surface energy balance surface model was used in conjunction with the projection technique developed in [16] to account for the heterogeneity of vegetation cover, soil type, and atmospheric conditions.

The overall accuracy in the downscaled values was evaluated to 3% (vol.) for EF and 2% (vol.) for AEF under cloud-free conditions. The projection was able to increase the correlation coefficient between SMI and surface soil moisture from 0.66 to 0.79 and from 0.71 to 0.81 for EF and AEF, respectively. The comparison of EF and AEF indicates that AEF is more directly linked to surface soil moisture, particularly for high soil moisture values. The diurnal variability of EF, which is due to temporal changes in incoming radiation and relative humidity, seems to explain the superiority of the AEF-based approach.

The main limitations to applying this approach to SMOS-sized pixels (about 40 km) globally are as follows: 1) It will be limited to clear-sky conditions; 2) it only works well for dry-end soil moisture contents; and 3) the availability of soil and vegetation parameters at high resolution. A sensitivity analysis of the method found that an error of 20% (vol.) in SMI observations had an effect of about 5% to 10% (vol.) on the downscaled soil moisture, depending on soil moisture and LAI values. However, the random uncertainty in a single measurement could be reduced by aggregating the SMI estimates. A given bias on the low-resolution soil moisture observation linearly impacted the downscaled soil moisture by the same amount, but random independent errors in input data cancelled out in the disaggregation results.

In this paper, ground-based, instead of remotely sensed, SMIs were used, and the extent of the data set ($\sim$10 km) was significantly smaller than the SMOS pixel. It is important to note that the spatial variability of micrometeorological data at the 40-km scale will be a limitation of the method. The spatial organization of meteorological forcing at 40-km scale will need to be assessed with data sets over larger areas. In addition, the dependence of the used SMIs to plant transpiration was assumed to be explained by vegetation cover (e.g., LAI) only. In particular, the impact of spatially variable vegetation stress on SMIs was neglected in this paper. Note that the sensitivity of thermal data to root-zone soil moisture over densely vegetated surfaces [40] and the decoupling under dry conditions between surface and deeper soil moisture [41] are likely to affect the performance of the method if these effects are not taken into account.

These results illustrate the potential of using high-resolution satellite-based estimates of instantaneous evapotranspiration obtained on clear-sky days for downscaling the coarse-resolution passive-microwave soil moisture. Recent studies have investigated the use of 1-km-resolution optical data, such as NOAA/AVHRR and MODIS, to develop operational schemes for monitoring EF at regional and global scales [27]–[29]. High-resolution microwave data collected during field experiments, such as the National Airborne Field Experiment [39], will be essential in testing this downscaling method for SMOS-sized areas in preparation for receiving SMOS data.

ACKNOWLEDGMENT

The authors would like to thank W. Kustas, D. Goodrich, S. Moran, and T. Schmugge for making the Monsoon'90 data available. The authors would also like to thank the USDA-ARSSWRC staff in Tombstone and Tucson for the past and current support and NASA and the USDA for the necessary financial support to conduct the Monsoon'90 field experiment. This included funds from NASA Interdisciplinary Research Program in Earth Sciences (NASA Reference IDP-88-086) and funds from the USDA-ARS Beltsville Area Office.

REFERENCES

[1] A. Western, R. Grayson, and T. Green, "The Tarrawarra project: High resolution spatial measurement, modelling and analysis of soil moisture and hydrological response," *Hydrol. Process.*, vol. 13, no. 5, pp. 633–652, 1999.

[2] A. Chehbouni, R. Escadafal, G. Boulet, B. Duchemin, V. Simmonaux, G. Dedieu, B. Mougenot, S. Khabba, H. Kharrou, O. Merlin, A. Chaponnière, J. Ezzahar, S. Erraki, J. Hoedjes, R. Hadria, H. Abourida, A. Cheggour, F. Raibi, L. Hanich, N. Guemouria, A. Chehbouni, A. Olioso, F. Jacob, and J. Sobrino, "The use of remotely sensed data for integrated hydrological modeling in arid and semi-arid regions: The SUDMED program," *Int. J. Remote Sens.*. submitted for publication. AQ4

[3] M. A. Perry and J. D. Niemann"Analysis and estimation of soil moisture at the catchment scale using EOFs," *J. Hydrol.*, vol. 334, no. 3/4, pp. 388–404, Feb. 2007.

[4] M. S. Moran, C. D. Peters-Lidard, J. M. Watts, and S. McElroy, "Estimating soil moisture at the watershed scale with satellite-based radar and land surface models," *Can. J. Remote Sens.*, vol. 30, no. 5, pp. 805–826, 2004.

[5] W. Wagner, G. Bloschl, P. Pampaloni, J.-C. Calvet, B. Bizzarri, J.-P. Wigneron, and Y. Kerr, "Operational readiness of microwave remote sensing of soil moisture for hydrologic applications," *Nordic Hydrol.*, vol. 38, no. 1, pp. 1–20. AQ5

[6] E. Njoku, E. Jackson, V. Lakshmi, T. Chan, and S. Nghiem, "Soil moisture retrieval from AMSR-E," *IEEE Trans. Geosci. Remote Sens.*, vol. 41, no. 2, pp. 215–229, Feb. 2003.

[7] T. J. Schmugge, "Applications of passive microwave observations of surface soil moisture," *J. Hydrol.*, vol. 212/213, pp. 188–197, 1998.

[8] Y. H. Kerr, P. Waldteufel, J.-P. Wigneron, J.-M. Martinuzzi, J. Font, and M. Berger, "Soil moisture retrieval from space: The soil moisture and ocean salinity (SMOS) mission," *IEEE Trans. Geosci. Remote Sens.*, vol. 39, no. 8, pp. 1729–1735, Aug. 2001.

[9] J.-P. Wigneron, J.-C. Calvet, T. Pellarin, A. Van De Griend, M. Berger, and P. Ferrazzoli, "Retrieving near surface soil moisture from microwave radiometric observations: Current status and future plans," *Remote Sens. Environ.*, vol. 85, no. 4, pp. 489–506, Jun. 2003.

[10] K. Saleh, J.-P. Wigneron, J.-P. Waldteufel, P. de Rosnay, J.-C. Calvet, and Y. Kerr, "Estimates of surface soil moisture under grass covers using L-band radiometry," *Remote Sens. Environ.*, vol. 109, no. 1, pp. 42–53, Jul. 2007.

[11] D. Entekhabi, G. R. Asrar, A. K. Betts, K. J. Beven, R. L. Bras, C. J. Duffy, T. Dunne, R. D. Koster, D. P. Lettenmaier, D. B. McLaughlin, W. J. Shuttleworth, M. T. van Genuchten, M.-Y. Wei, and E. F. Wood, "An agenda for land surface hydrology research and a call for the second international hydrological decade," *Bull. Amer. Meteorol. Soc.*, vol. 80, no. 10, pp. 2043–2058, 1999.

[12] O. Merlin, A. Chehbouni, G. Boulet, and Y. Kerr, "Assimilation of disaggregated microwave soil moisture into a hydrologic model using coarse-scale meteorological data," *J. Hydrometeorol.*, vol. 7, no. 6, pp. 1308–1322, 2006.

[13] J. Pellenq, J. Kalma, G. Boulet, G.-M. Saulnier, S. Wooldridge, Y. Kerr, and A. Chehbouni, "A disaggregation scheme for soil moisture based on topography and soil depth," *J. Hydrol.*, vol. 276, no. 1–4, pp. 112–127, May 2003.

[14] X. Zhan, P. R. Houser, J. P. Walker, and W. Crow, "A method for retrieving high resolution surface soil moisture from hydros L-band radiometer and radar observations," *IEEE Trans. Geosci. Remote Sens.*, vol. 44, no. 6, pp. 1534–1544, Jun. 2006. DOI:10.1109/TGRS.2005.863319.

[15] N. S. Chauhan, S. Miller, and P. Ardanuy, "Spaceborne soil moisture estimation at high resolution: A microwave-optical/IR synergistic approach," *Int. J. Remote Sens.*, vol. 24, no. 22, pp. 4599–4622, 2003.

[16] O. Merlin, A. Chehbouni, Y. Kerr, E. G. Njoku, and D. Entekhabi, "A combined modeling and multi-spectral/multi-resolution remote sensing approach for disaggregation of surface soil moisture: Application to SMOS configuration," *IEEE Trans. Geosci. Remote Sens.*, vol. 43, no. 9, pp. 2036–2050, Sep. 2005.

[17] W. P. Kustas, D. C. Goodrich, M. S. Moran, S. A. Amer, L. B. Bach, J. H. Blanford, A. Chehbouni, H. Claassen, W. E. Clements, P. C. Doraiswamy, P. Dubois, T. R. Clarke, C. S. T. Daughtry, D. I. Gellman, T. A. Grant, L. E. Hipps, A. R. Huete, K. S. Humes, T. J. Jackson, T. O. Keefer, W. D. Nichols, R. Parry, E. M. Perry, R. T. Pinker, P. J. Pinter, J. Qi, A. C. Riggs, T. J. Schmugge, A. M. Shutko, D. I. Stannard, E. Swiatek, J. D. van Leeuwen, J. van Zyl, A. Vidal, J. Washburne, and M. A. Weltz, "An interdisciplinary field study of the energy and water fluxes in the atmosphere-biosphere system over semiarid rangelands: Description of some preliminary results," *Bull. Amer. Meteorol. Soc.*, vol. 72, no. 11, pp. 1683–1705, Nov. 1991.

[18] W. P. Kustas and D. C. Goodrich, "Monsoon '90 multidisciplinary experiment," *Water Resour. Res.*, vol. 30, no. 5, pp. 1211–1225, 1994.

[19] T. Schmugge, T. J. Jackson, W. P. Kustas, R. Roberts, R. Parry, D. C. Goodrich, S. A. Amer, and M. A. Weltz, "Push broom microwave radiometer observations of surface soil moisture in Monsoon '90," *Water Resour. Res.*, vol. 30, no. 5, pp. 1321–1328, 1994.

[20] W. J. Shutlleworth, R. J. Gurley, A. Y. Hsu, and J. P. Ormsby, "FIFE: The variation in energy partition at surface flux sites," *IAHS Publ.*, vol. 186, pp. 67–74, 1989.

[21] M. Sugita and W. Brutsaert, "Daily evaporation over a region from lower boundary-layer profiles measured with radiosondes," *Water Resour. Res.*, vol. 27, no. 5, pp. 742–752, 1991.

[22] R. D. Crago, "Conservation and variability of the evaporative fraction during the daytime," *J. Hydrol.*, vol. 180, no. 1, pp. 173–194, May 1996.

[23] R. Crago and W. Brutsaert, "Daytime evaporation and the self-preservation of the evaporative fraction and the Bowen ratio," *J. Hydrol.*, vol. 178, no. 1, pp. 241–255, Apr. 1996.

[24] P. Gentine, D. Entekhabi, A. Chehbouni, G. Boulet, and B. Duchemin, "Analysis of diurnal evaporative fraction behavior," presented at the 83th AMS Annu. Meeting, Atlanta, GA, Feb. 2006. 28-3.

[25] W. P. Kustas, T. J. Schmugge, K. S. Humes, T. J. Jackson, and R. Parry, "Relationships between evaporative fraction and remotely sensed vegetation index and microwave brightness temperature for semiarid rangelands," *J. Appl. Meteorol.*, vol. 32, no. 12, pp. 1781–1790, Dec. 1993.

[26] K. Nishida, R. R. Nemani, S. W. Running, and J. M. Glassy, "An operational remote sensing algorithm of land surface evaporation," *J. Geophys. Res.*, vol. 108, no. D9, p. 4270, 2003. DOI:10.1029/2002JD002062.

[27] L. Jiang and S. Islam, "Estimation of surface evaporation map over southern great plains using remote sensing data," *Water Resour. Res.*, vol. 37, no. 2, pp. 329–340, 2001.

[28] K. Nishida, R. R. Nemani, J. M. Glassy, and S. W. Running, "Development of an evapotranspiration index from Aqua/MODIS for monitoring surface moisture status," *IEEE Trans. Geosci. Remote Sens.*, vol. 41, no. 2, pp. 493–501, Feb. 2003.

[29] K. Wang, Z. Li, and M. Cribb, "Estimation of evaporative fraction from a combination of day and night land surface temperatures and NDVI: A new method to determine the Priestley-Taylor parameter," *Remote Sens. Environ.*, vol. 102, no. 3/4, pp. 293–305, Jun. 2006.

[30] M. A. Weltz, J. C. Ritchie, and H. D. Fox, "Comparison of laser and field measurements of vegetation height and canopy cover," *Water Resour. Res.*, vol. 30, no. 5, pp. 1311–1319, 1994.

[31] J. M. Norman, W. P. Kustas, and K. S. Humes, "Source approach for estimating soil and vegetation energy fluxes in observations of directional radiometric surface temperature," *Agric. For. Meteorol.*, vol. 77, no. 3, pp. 263–293, Dec. 1995.

[32] W. P. Kustas, X. Zhan, and T. J. Schmugge, "Combining optical and microwave remote sensing for mapping energy fluxes in a semiarid watershed," *Remote Sens. Environ.*, vol. 64, no. 2, pp. 116–131, May 1998.

[33] W. P. Kustas and J. M. Norman, "Evaluation of soil and vegetation heat flux predictions using a simple two-source model with radiometric temperatures for partial canopy cover," *Agric. For. Meteorol.*, vol. 94, no. 1, pp. 13–29, Apr. 1999.

[34] P. J. Sellers, M. D. Heiser, and F. G. Hall, "Relations between surface conductance and spectral vegetation indices at intermediate (100 m^2 to 15 km^2) length scales," *J. Geophys. Res.*, vol. 97, no. D17, pp. 19 033–19 059, 1992.

[35] K. E. Saxton, W. J. Rawls, J. S. Romberger, and R. I. Papendick, "Estimating generalized soil-water characteristics from texture," *Soil Sci. Soc. Amer. J.*, vol. 50, no. 4, pp. 1031–1036, 1986.

[36] T. S. Komatsu, "Toward a robust phenomenological expression of evaporative efficiency for unsaturated soil surfaces," *J. Appl. Meteorol.*, vol. 42, no. 9, pp. 1330–1334, 2003.

[37] J.-P. Lhomme and E. Elguero, "Examination of evaporative fraction diurnal behaviour using a soil-vegetation model coupled with a mixed-layer model," *Hydrol. Earth Syst. Sci.*, vol. 3, no. 2, pp. 259–270, 1999.

[38] J. L. Champeaux, V. Masson, and F. Chauvin, "ECOCLIMAP: A global database of land surface parameters at 1 km resolution," *Meteorol. Appl.*, vol. 12, no. 1, pp. 29–32, Mar. 2005.

[39] R. Panciera, J. Walker, J. Kalma, E. Kim, J. Hacker, O. Merlin, M. Berger, and N. Skou, "The NAFE'05/CoSMOS data set: Towards SMOS calibration, downscaling and assimilation," *IEEE Trans. Geosci. Remote Sens.*, vol. 46, no. 3, Mar. 2008.

[40] W. T. Crow, W. Kustas, and J. H. Prueger, "Monitoring root-zone soil moisture through the assimilation of a thermal remote sensing-based soil moisture proxy into a water balance model," *Remote Sens. Environ.*, 2007. **AQ6** in press.

[41] W. J. Capehart and T. N. Carlson, "Decoupling of surface and near-surface soil water content: A remote sensing perspective," *Water Resour. Res.*, vol. 33, no. 6, pp. 1383–1395, 1997.

Olivier Merlin received the engineering degree in nuclear physics from the Ecole Nationale Supérieure de Physique de Grenoble, Grenoble, France, in 2000 and the Master's degree in techniques for space from the Ecole Nationale Supérieure de l'Aéronautique et de l'Espace, Toulouse, France, in 2001. He is currently working toward the Ph.D. degree at the Centre d'Etudes Spatiales de la Biosphère, Toulouse.

Abdelghani Chehbouni received the Ph.D. degree in hydrology and remote sensing from the University Paul Sabatier, Toulouse, France, in 1992.

He was with the University of Arizona, Tucson, for 18 months and with the Jet Propulsion Laboratory, Pasadena, CA, for two years. He is currently a Research Scientist with the IRD-CESBIO, which has been part of the Centre d'Etudes Spatiales de la Biosphère (CESBIO), Toulouse, since 1992, where he is currently a Leader of the hydrology group that is in charge of a project dealing with land degradation, climate change, and water resources in Morocco. He is a Coinvestigator of several remote sensing programs (VEGETATION, ERS2/ATSR2, EOS, and SMOS). He is participating in several international experiments (MONSOON'90, Hapex Sahel) and is a Coleader of the Semi-Arid-Land-Surface-Atmosphere international program. His main research interests include the application of remotely sensed data in land surface–atmosphere models, particularly in arid and semiarid regions. **AQ7**

Jeffrey P. Walker received the B.Surv. and B.E. (civil) degrees from the University of Newcastle, Australia, in 1995 and the Ph.D. degree in environmental engineering from the same university in 1999.

He was with the Hydrological Sciences Branch, NASA Goddard Space Flight Center, as a Visiting Scientist for two years before joining the Department of Civil and Environmental Engineering, University of Melbourne, Melbourne, Australia. His research has been focused on environmental sensing, earth system modeling, and data assimilation.

Rocco Panciera photograph and biography not available at the time of publication. **AQ8**

Yann Kerr (M'88–SM'01) received the engineering degree in radar and telecommunications from the Ecole Nationale Supérieure de l'Aéronautique et de l'Espace, Toulouse, France, the M.Sc. degree in electronics and electrical engineering from Glasgow University, Glasgow, U.K., and the Ph.D. degree in remote sensing and hydrology from the Université Paul Sabatier, Toulouse.

From 1980 to 1985, he was with the Centre National d'Etudes Spatiales, Toulouse. In 1985, he was with the Laboratoire d'Etudes et de Recherches en Télédétection Spatiale, Toulouse, as a Research Scientist. From May 1987 to December 1988, he was on leave of absence to work with the Jet Propulsion Laboratory, California Institute of Technology, Pasadena. He is currently with the Centre d'Etudes Spatiales de la Biosphère, Toulouse. His fields of interest are in the theory and techniques for microwave and thermal infrared remote sensing of the Earth, with emphasis on hydrology and vegetation monitoring. He is currently the Lead Investigator of the ESA/CNES/CDTI Earth Explorer Opportunity Soil Moisture and Ocean Salinity mission, which is currently in phase C/D, and is a Coinvestigator on the NASA ESSP HYDROS mission.

AUTHOR QUERIES

AUTHOR PLEASE ANSWER ALL QUERIES

AQ1 = “in % vol.” was expanded as “in volume percent”. Please check if appropriate.
AQ2 = “saturation vapor pressure temperature relationship” was changed to “saturation vapor pressure versus temperature relationship”. Please check if appropriate.
AQ3 = The sentence was reworded. Please check if appropriate.
AQ4 = Please provide publication update in Ref. [2].
AQ5 = Please provide year of publication in Ref. [5].
AQ6 = Please provide publication update in Ref. [40].
AQ7 = “land-surface atmosphere models” was changed to “land surface-atmosphere models”. Please check if appropriate.
AQ8 = Please provide photograph and biography of author R. Panciera.

Notes: 1) Bios were taken from the IEEE explore. Please update.
2) Please provide photograph for all authors (if available).

END OF ALL QUERIES